Determination of Size and Concentration of Gold Nanoparticles from Extinction Spectra

ARTICLE *in* ANALYTICAL CHEMISTRY · SEPTEMBER 2008

Impact Factor: 5.64 · DOI: 10.1021/ac800834n · Source: PubMed

1 AUTHOR:

Nikolai G. Khlebtsov
Institute of Biochemistry and Physiology of…

229 PUBLICATIONS **4,827** CITATIONS

SEE PROFILE

Anal. Chem. **2008,** *80,* 6620–6625

Determination of Size and Concentration of Gold Nanoparticles from Extinction Spectra

Nikolai G. Khlebtsov*

Institute of Biochemistry and Physiology of Plants and Microorganisms, Russian Academy of Sciences, 13 Prospekt Entuziastov, Saratov 410049, Russia, and Saratov State University, 83 Ulitsa Astrakhanskaya, Saratov 410026, Russia

Extinction spectra of colloidal gold can be used for a simple and fast determination of the size and concentration of nanoparticles. It is generally accepted that experimental correlations of the particle size and concentration with the plasmon resonance properties are in agreement with Mie theory simulations. Here, we discuss this point in the context of a long-term collection of published experimental data and our T-matrix simulations, which account for deviations of the particle size from ideal monodisperse spheres. These deviations result in small but quite evident disagreements between the Mie calculations and the experimental calibration curves "particle size vs resonance wavelength". We present a long-term-averaged analytical particle-size calibration and also discuss the effects of the particle dielectric functions, shape and size polydispersity on simulated correlations between the extinction spectra and the average particle size, and concentration.

In the past few years, gold nanoparticles (NPs)[1] have attracted interest as a novel platform for various applications to nanobiotechnology[2] and nanomedicine[3] because of convenient surface bioconjugation with molecular probes and remarkable plasmon-resonant optical properties.[4] Recently published examples include applications of NPs to biosensorics,[5] genomics,[6] clinical chemistry,[7] immunoassays,[8] optical imaging of biological cells (including cancer cell imaging with resonance scattering,[9] optical coherence tomography,[10] two-photon luminescence,[11] and photoacoustic[12] techniques), targeted drug delivery,[13] immune response enhancement,[14] and cancer cell photothermolysis.[15] Most of these examples are based on a combination of biological recognition (the probe molecule + the target molecule) and resonance absorption or scattering of light on frequencies corresponding to excitation of localized plasmons.[16] Moreover, molecular recognition has recently been used for a DNA-programmable formation of nanoparticle methacrystals.[17]

Accurate determination of the size and concentration of NPs is essential for most biomedical applications of NPs. For instance, size and concentration are crucial parameters determining the uptake of NPs by living cells[18] and their circulation and biodistribution in living bodies.[19] Whereas TEM is a reliable method for the sizing of metal NPs, there are no analogous time-tested and convenient tools for concentration measurements. In the routine laboratory practice, it would be desirable to have a simple,

* Contact information. E-mail: khlebtsov@ibppm.sgu.ru.

(1) Daniel, M. C.; Astruc, D. *Chem. Rev.* **2004**, *104*, 293–346.
(2) Cheng, M. M.; Cuda, G.; Bunimovich, Y. L.; Gaspari, M.; Heath, J. R.; Hill, H. D.; Mirkin, C. A.; Nijdam, A. J.; Terracciano, R.; Thundat, T.; Ferrari, M. *Curr. Opin. Chem. Biol.* **2006**, *10*, 11–19.
(3) Liao, H.; Nehl, C. L.; Hafner, J. H. *Nanomedicine* **2006**, *1*, 201–208.
(4) Kreibig, U.; Vollmer, M. *Optical Properties of Metal Clusters*; Springer-Verlag: Berlin, Germany, 1995.
(5) Katz, E.; Willner, I. *Angew. Chem., Int. Ed.* **2004**, *43*, 6042–6108. Wei, A. *e-J. Surf. Sci. Nanotech.* **2006**, *4*, 9–18. Stewart, M. E.; Anderton, Ch. R.; Thompson, L. B.; Maria, J.; Gray, S. K.; Rogers, J. A.; Nuzzo, R. G. *Chem. Rev.* **2008**, *108*, 494–521.
(6) Rosi, N. L.; Mirkin, C. A. *Chem. Rev.* **2005**, *105*, 1547–1562. Doria, G.; Franco, R.; Baptista, P. *IET Nanobiotechnol.* **2007**, *1*, 53–57. Liu, X.; Dai, Q.; Austin, L.; Coutts, J.; Knowles, G.; Zou, J.; Chen, H.; Huo, Q. *J. Am. Chem. Soc.* **2008**, *130*, 2780–2782.
(7) Baptista, P. V.; Koziol-Montewka, M.; Paluch-Oles, J.; Doria, G.; Franco, R. *Clin. Chem.* **2006**, *52*, 1433–1434.
(8) Baptista, P.; Pereira, E.; Eaton, P.; Doria, G.; Miranda, A.; Gomes, I.; Quaresma, P.; Franco, R. *Anal. Bioanal. Chem.* **2008**, DOI 10.1007/s00216-007-1768-z. Gupta, Sh.; Huda, S.; Kilpatrick, P. K.; Velev, O. D. *Anal. Chem.* **2007**, *79*, 3810–3820. Hou, S.-Y.; Chen, H.-K.; Cheng, H.-C.; Huang, C.-Y. *Anal. Chem.* **2007**, *79*, 980–985.
(9) El-Sayed, I. H.; Huang, X.; El-Sayed, M. A. *Nano Lett.* **2005**, *5*, 829–834. Aaron, J.; Nitin, N.; Travis, K.; Kumar, S.; Collier, T.; Park, S. Y.; José-Yakamán, M.; Coghlan, L.; Follen, M.; Richards-Kortum, R.; Sokolov, K. *J. Biomed. Opt.* **2007**, *12*, 034007. (1−11). Aaron, J.; de la Rosa, E.; Travis, K.; Harrison, N.; Burt, J.; José-Yakamán, M.; Sokolov, K. *Opt. Express* **2008**, *16*, 2153–2167.
(10) Loo, C.; Hirsch, L.; Lee, M.; Chang, E.; West, J.; Halas, N.; Drezek, R. *Opt. Lett.* **2005**, *30*, 1012–1014.
(11) Kumar, S.; Harrison, N.; Richards-Kortum, R.; Sokolov, K. *Nano Lett.* **2007**, *7*, 1338–1343.
(12) Zharov, V.; Galanzha, E.; Shashkov, E.; Khlebtsov, N.; Tuchin, V. *Opt. Lett.* **2006**, *31*, 3623–3625. Mallidi, S.; Larson, T.; Aaron, J.; Sokolov, K.; Emelianov, S. *Opt. Express* **2007**, *15*, 6583–6588.
(13) Paciotti, G. F.; Kingston, D. G. I.; Tamarkin, L. *Drug Dev. Res.* **2006**, *67*, 47–54. Azzazy, H. M. E.; Mansour, M. M. H.; Kazmierczak, S. C. *Clin. Chem.* **2006**, *52*, 1238–1246.
(14) Dykman, L. A.; Bogatyrev, V. A. *Russ. Chem. Rev.* **2007**, *76*, 181–194.
(15) Huang, X.; El-Sayed, I. H.; Qian, W.; El-Sayed, M. A. *J. Am. Chem. Soc.* **2006**, *128*, 2115–2120. Pissuwan, D.; Valenzuela, S. M.; Cortie, M. B. *Trends Biotechnol.* **2006**, *24*, 62–67. Khlebtsov, B. N.; Zharov, V. P.; Melnikov, A. G.; Tuchin, V. V.; Khlebtsov, N. G. *Nanotechnology* **2006**, *17*, 5167–5179. Jain, P. K.; El-Sayed, I. H.; El-Sayed, M. A. *Nano Today* **2007**, *2*, 18–29.
(16) Kelly, K. L.; Coronado, E.; Zhao, L. L.; Schatz, G. C. *J. Phys. Chem. B* **2003**, *107*, 668–677.
(17) Nykypanchuk, D.; Maye, M. M.; van der Lelie, D.; Gang, O. *Nature* **2008**, *451*, 549–552. Park, S. Y.; Lytton-Jean, A. K.; Lee, B.; Weigand, S.; Schatz, G. C.; Mirkin, C. A. *Nature* **2008**, *451*, 553−−556.
(18) Chithrani, B. D.; Chan, W. C. W. *Nano Lett.* **2007**, *7*, 1542–1550. Giljohann, D. A.; Seferos, D. S.; Patel, P. C.; Millstone, J. E.; Rosi, N. L.; Mirkin, C. A. *Nano Lett.* **2007**, *7*, 3818–3821. Jiang, W.; Kim, B. Y. S.; Rutka, J. T.; Chan, W. C. W. *Nat. Nanotechnol.* **2008**, *3*, 145–150.
(19) De Jong, W. H.; Hagens, W. I.; Krystek, P.; Burger, M. C.; Sips, A. J. A. M.; Geertsma, R. E. *Biomaterials* **2008**, *29*, 1912–1919.

10.1021/ac800834n CCC: $40.75
Published on Web 07/22/2008

fast, and low-cost method for rapid monitoring of the NP size and concentration during all preparative stages, from NP synthesis to characterization of fabricated biomarkers (functionalized nanoparticles). In our opinion, standard UV−vis spectrophotometry ideally meets these goals (see, e.g., refs 1 and 20–22 and citations therein), in spite of the existence of alternative techniques such as dynamic light scattering,[23] static light scattering,[24] and so on.

Experimental correlations of the particle size and concentration with the extinction spectra of gold has been studied for a broad particle-size range (5−100 nm) in two recent reports.[25,26] In particular, Haiss et al.[25] presented a convenient set of calibration plots, formulas, and tables for fast determination of the gold NP size and concentration. Here, we discuss NP size and concentration measurements in relation to a long-term collection of published experimental data and our T-matrix simulations, which account for deviation of the particle size from ideal spheres. Our goal is to discuss possible disagreements between Mie calculations and experimental calibration curves of the type "NP size vs resonance wavelength" or "NP concentration vs resonance extinction or extinction ratios". We believe that such a discussion may be useful for researchers in their practical quantitative characterization of gold NPs with UV−vis spectrophotometry and in understanding of possible limitations related to deviations of the particle parameters from an ideal model of monodisperse Mie spheres.

THEORETICAL METHODS

The size-corrected dielectric functions of a spherical gold particle can be obtained by the well-known extended Drude model.[4,27] It is assumed that the interband contribution is independent of the particle size; so, the size-corrected dielectric function $\varepsilon_p(\lambda)$ is expressed as

$$\varepsilon_p(\lambda) = \varepsilon_b(\lambda) + \Delta\varepsilon(\lambda) \tag{1}$$

where ε_b is the bulk value; the correction $\Delta\varepsilon(\lambda)$ is determined by the difference between two Drude terms,

$$\Delta\varepsilon = \frac{\omega_p^{\,2}}{\omega^2 + i\omega/\tau_b} - \frac{\omega_p^{\,2}}{\omega^2 + i\omega/\tau_p} \tag{2}$$

with the bulk τ_b and modified $\tau_p^{-1} = \tau_b^{-1} + A_L v_F/L_{eff}$ electron mean free lifetimes or with the corresponding damping constants $\gamma_b = \tau_b^{-1}$ and $\gamma_p = \tau_p^{-1}$; ω_p is the plasma frequency; v_F is the Fermi velocity of free electrons; L_{eff} is the effective mean free path of electrons (for a sphere with a radius a, $L_{eff} \simeq a$); and the proportionality coefficient A_L can be considered to be a fitting parameter[28] close to 1. Numerical estimations[27] and a thorough comparison of the experimental and calculated colloidal gold spectra[20,29] showed that only the imaginary part of the bulk metal permittivity ε_b'' should be corrected (see below):

$$\varepsilon_p''(\lambda) \simeq \varepsilon_b'' + A_L \frac{\lambda_p}{L_{eff}} \left(\frac{v_F}{2\pi c}\right) \left(\frac{\lambda}{\lambda_p}\right)^3 \tag{3}$$

where L_{eff} is the effective mean free path of electrons, λ_p is the wavelength of plasma oscillations, and c is the light velocity in vacuum.

Such an isotropic and a homogeneous modification of the bulk dielectric function can also be applied to an arbitrarily shaped and structured particle according to the generalizations of eq 1 given by Coronado and Schatz[30] and by Liu and Guyot-Sionnest.[31] Specifically, the parameter τ_p of a particle is determined by an effective electron free path $L_{eff} = 4V/S$, as expressed in terms of the particle volume V and the surface S. In light of the recent single-particle experiments,[32] the size-limiting effects in nanoparticle optics have been discussed in a recent excellent review.[33]

There exist several sets of the bulk Au optical constants for polycrystalline films[34–37] and for monocrystalline samples.[38] The data by Hageman et al.[36] satisfy the Kramers−Kronig relations[27] and agree with the measurements by Canifeld et al.[37] At present, the data by Johnson and Christy[39] are the most popular and are widely used in almost all simulations published recently. Figure 1 shows the spectral dependence of the real and imaginary parts of the refractive index taken from different sources, together with a spline obtained by analogy with ref 24. Specifically, the spline nods for the 210−470, 480−640, and 640−1605 nm spectral bands were taken from refs 35, 38, and 39, respectively. For the most important plasmon-resonant band, 480−640 nm, we chose Otter's[38] data in accordance with the recommendation by Doremus[40] and our observations,[20] indicating that the Otter's constants give the

(20) Khlebtsov, N. G.; Bogatyrev, V. A.; Dykman, L. A.; Melnikov, A. G. *J. Colloid Interface Sci.* **1996**, *180*, 436–445.
(21) Mulvaney, P. *Langmuir* **1996**, *12*, 788–800.
(22) Brown, K. R.; Walter, D. G.; Natan, M. J. *Chem. Mater.* **2000**, *12*, 306–313.
(23) Berne, B. J.; Pecora R. *Dynamic Light Scattering: With Application to Chemistry, Biology, and Physics*; Dover Publ.: Mineola, NY, 2002.
(24) Khlebtsov, N. G.; Bogatyrev, V. A.; Dykman, L. A.; Khlebtsov, B. N.; Krasnov, Ya. M. *J. Quant. Spectrosc. Radiat. Transfer* **2004**, *89*, 133–142.
(25) Haiss, W.; Thanh, N. T. K.; Aveard, J.; Fernig, D. G. *Anal. Chem.* **2007**, *79*, 4215–4221.
(26) Njoki, P. N.; Lim, I.-I. S.; Mott, D.; Park, H.-Y.; Khan, B.; Mishra, S.; Sujakumar, R.; Luo, J.; Zhong, C.-J. *J. Phys. Chem. B* **2007**, *111*, 14664–14669.
(27) Bohren, C. F.; Huffman, D. R. *Absorption and Scattering of Light by Small Particles*; John Wiley & Sons: New York, 1983.
(28) Quinten, M. *Z. Phys. B* **1996**, *101*, 211–217.
(29) Scaffardi, L. B.; Pellegri, N.; de Sanctis, O.; Tocho, J. O. *Nanotechnology* **2005**, *16*, 158–163.
(30) Coronado, E. A.; Schatz, G. C. *J. Chem. Phys.* **2003**, *119*, 3926–3934.
(31) Liu, M.; Guyot-Sionnest, P. *J. Phys. Chem. B* **2004**, *108*, 5882–5888.
(32) Sönnichsen, C.; Franzl, T.; Wilk, T.; von Plessen, G.; Feldmann, J.; Wilson, O.; Mulvaney, P. *Phys. Rev. Lett.* **2002**, *88*, 077402−077405. Novo, C.; Gomez, D.; Perez-Juste, J.; Zhang, Z.; Petrova, H.; Reismann, M.; Mulvaney, P.; Hartland, G. V. *Phys. Chem. Chem. Phys.* **2006**, *8*, 3540–3546. Nehl, C. L.; Grady, N. K.; Goodrich, G. P.; Tam, F.; Halas, N. J.; Hafner, J. H. *Nano Lett.* **2004**, *4*, 2355–2359. Arbouet, A.; Christofilos, D.; Del Fatti, N.; Vallée, F.; Huntzinger, J. R.; Arnaud, L.; Billaud, P.; Broyer, M. *Phys. Rev. Lett.* **2004**, *93*, 127401. (1−4). Muskens, O. L.; Del Fatti, N.; Vallée, F.; Huntzinger, J. R.; Billaud, P.; Broyer, M. *Appl. Phys. Lett.* **2006**, *88*, 0634109.
(33) Hu, M.; Novo, C.; Funston, A.; Wang, H.; Staleva, H.; Zou, S.; Mulvaney, P.; Xia, Y.; Hartland, G. V. *J. Mater. Chem.* **2008**, *18*, 1949–1960.
(34) Schulz, L. G. *J. Opt. Soc. Am.* **1954**, *44*, 357–362. Schulz, L. G.; Tangherlini, F. R. *J. Opt. Soc. Am.* **1954**, *44*, 362–368.
(35) Irani, G. B.; Huen, T.; Wooten, F. *J. Opt. Soc. Am.* **1971**, *61*, 128–129.
(36) Hagemann, H.-J.; Gudat, W.; Kunz, C. Optical Constants from the Far Infrared to the X-ray Region: Mg, Al, Cu, Ag, Au, Bi, C, and Al_2O_3. Deutsches Elektronen-Synchrotron, DESY Int. Report No. SR-74/7, Hambug, Germany, 1974. Hagemann, H.-J.; Gudat, W.; Kunz, C. *J. Opt. Soc. Am.* **1975**, *65*, 742–744.
(37) Canifeld, L. R.; Hass, G.; Hunter, W. R. *J. Phys. (Paris)* **1964**, *25*, 124–129.
(38) Otter, M. Z. *Physik* **1961**, *161*, 163–178.
(39) Johnson, P. B.; Christy, R. W. *Phys. Rev. B* **1972**, *6*, 4370–4379.
(40) Doremus, R. H. *J. Chem. Phys.* **1964**, *40*, 2389–2396.

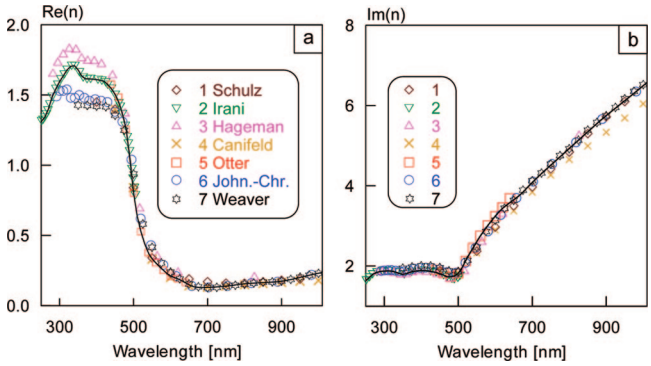

Figure 1. Spectral dependence of the real (a) and imaginary (b) parts of the refractive index of bulk gold, according to the data of refs 34– 39, 42 (symbols 1−7, respectively). The solid curve shows the Sp1 spline (see text).

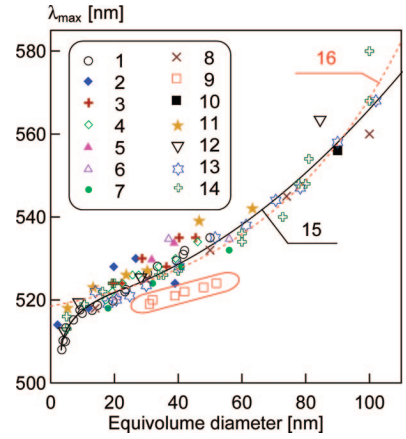

Figure 2. Position of the surface plasmon resonance peak (λ_{max}) as a function of the mean equivolume particle diameter for gold NPs in water. The symbols designate experimental data taken from the following works: 1, ref 20; 2−5, ref 22; 6 and 7, ref 47; 8, ref 48; 9, ref 49; 10, ref 52; 11, ref 50; 12, ref 51; 13, ref 26; 14, ref 25. Solid line 15 was calculated by eq 4; dashed line 16 corresponds to eq 9 in ref 25. Note that the data of ref 49 (□, circled selection) are in evident disagreement with the majority of points and both calibrations.

best agreement between the measured and the calculated resonance wavelength. In the short-wavelength part, Irani's[35] data seem most reliable (Figure 1), whereas for 650−1600 nm, we used the tabulated data of Johnson and Christy.[39] For simplicity, this spline will be designated Sp1. For some comparisons, we also used a spline based directly on Johnson and Christy's[39] data, designated Sp2. For each spline, two variants of size correction are possible. One involved a complete size-correction procedure by eqs 1 and 2 for both the real and the imaginary part of the refractive index $n = \varepsilon_p^{1/2}$. In the other variant, we put $\Delta\varepsilon \equiv \mathrm{Re}(\Delta\varepsilon') = 0$ and corrected only the imaginary part of the dielectric function, according to eq 3. Underwood and Mulvaney[41] found that the ε'_b values of Johnson and Christy[39] were more accurate in predictions of surface plasmon resonance wavelengths but that ε''_b was more accurately provided by Weaver et al.[42] Accordingly, we included in our consideration the dielectric data of ref 42.

The optical properties of a particle with an equivolume radius $a_{ev} = d_{ev}/2$ can be expressed in terms of the extinction cross section $C_{ext} = \pi a_{ev}^2 Q_{ext}$, which defines the extinction $A_{ext} = \lg(e) l N C_{ext}$ of an ensemble of N randomly oriented particles (per 1 cm^3; the optical path equals l [cm]) with the same volume and shape. Generally, the extinction cross section should be averaged over particle size and shape distributions and over orientations. In this work, we considered spherical particles (radius, a) and circular cylinders (s-cylinders[43]) with semispherical ends, which are characterized by the thickness of $2b$, the length of $2a$, and the aspect ratio of $e = a/b$. Such a model gives a reasonable fit to TEM images and to deviations of the particle shape from spheres.[20,22] To calculate the extinction cross section of spheres and randomly oriented s-cylinders in water, we used standard Mie codes[27] and our T-matrix codes for randomly oriented particles, as described in ref 43.

RESULTS AND DISCUSSION

Earlier,[20] we proposed a calibration curve for determination of the equivolume diameter $5 \le d_{ev}(\mathrm{nm}) \le 50$ of NPs obtained by the citrate method of Frens.[44] This calibration has been checked in independent studies.[45,46] Here, we extend our consideration to the $5 \le d_{ev}(\mathrm{nm}) \le 100$ region. Figure 2 shows a long-term collection of experimental measurements of the extinction resonance position as a function of the mean equivolume particle diameter. The sources of experimental data[20,22,25,26,47–52] are indicated in the figure caption. Solid line 15 in Figure 2 represents an averaged calibration curve, which is described by the following equation:

$$d = \begin{cases} 3 + 7.5\times10^{-5}X^4, X < 23 \\ [\sqrt{X-17}-1]/0.06, X \ge 23 \end{cases}, \quad X = \lambda_{max} - 500 \qquad (4)$$

where all quantities are expressed in nanometers. This equation should be considered as an empirical generalization of a large volume of experimental data, which effectively account for deviations of the particle shape from sphericity.

Dashed line 16 in Figure 2 shows a calibration curve calculated by eq 9 of Haiss et al.[25] In general, both calibrations are in close agreement except for the small-particle region $d < 20$ nm. In spite of the evident distribution of experimental points around our analytical curve, there is some general agreement between the data of different authors, with the only evident exception. Specifically, the data of Andreescu et al.[49] (selected squares in Figure

(41) Underwood, S.; Mulvaney, P. *Langmuir* **1994**, *10*, 3427–3430.
(42) Weaver, J. H., Krafka, C., Lynch, D. W., Koch, E. E., Eds. *Optical Properties of Metals* , Vol. 2; Physics Data Series No. 18-2, Fachinformationszentrum Karlsruhe: Kalsruhe, Germany, 1981.
(43) Alekseeva, A. V.; Bogatyrev, V. A.; Dykman, L. A.; Khlebtsov, B. N.; Trachuk, L. A.; Melnikov, A. G.; Khlebtsov, N. G. *Appl. Opt.* **2005**, *44*, 6285–6295.
(44) Frens, G. *Nat. Phys. Sci.* **1973**, *241*, 20–22.
(45) Nowicki, W. *Colloids Surf., A* **2001**, *194*, 159–173.
(46) Doron, A.; Joselevich, E.; Schlittner, A.; Willner, I. *Thin Solid Films* **1999**, *340*, 183–188.
(47) Brown, K. R.; Natan, M. J. *Langmuir* **1998**, *14*, 726–728.
(48) Chithrani, B. D.; Ghazani, A. A.; Chan, W. C. W. *Nano Lett.* **2006**, *6*, 662–668.
(49) Andreescu, D.; Sau, T. K.; Goia, D. V. *J. Colloid Interface Sci.* **2006**, *298*, 742–751.
(50) Horisberger, M. In *Techniques in Immunocytochemistry* Bullock, G. R., Petrusz P., Eds.; Academic Press: London, U.K., 1985; p 155.
(51) Slouf, M.; Kuzel, R.; Matej, Z. *Z. Kristallogr. Suppl.* **2006**, *23*, 319–324.
(52) Alekseeva, A. V.; Bogatyrev, V. A.; Khlebtsov, B. N.; Melnikov, A. G.; Dykman, L. A.; Khlebtsov, N. G. *Colloid J.* **2006**, *68*, 661–678.

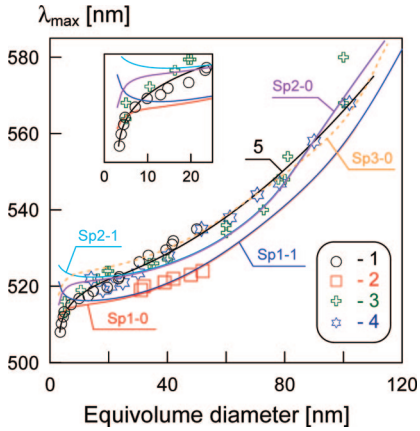

Figure 3. The same as in Figure 2 but with experimental data: 1, ref 20; 2, ref 49; 3, ref 25; and 4, ref 26. Solid line 5 was calculated by eq 4; the other lines were calculated by Mie theory. Symbols Sp1-0 and Sp1-1 designate calculations with the optical-constant Sp1 and with the real part $\Delta\varepsilon' = 0$ and $\Delta\varepsilon' \neq 0$, respectively. Symbols Sp2-0 and Sp2-1 correspond to Johnson–Christy's[39] optical constants with $\Delta\varepsilon' = 0$ and $\Delta\varepsilon' \neq 0$. The symbol Sp3-0 corresponds to Weaver et al.'s[42] optical constants with $\Delta\varepsilon' = 0$. The inset shows an enlarged part of the plots for small diameters.

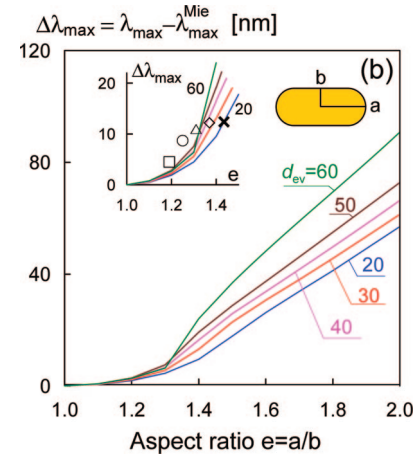

Figure 4. Deviations of the extinction peak positions of gold s-cylinders from Mie theory as a function of the particle aspect ratio. Calculations by the T-matrix method for particles with equivolume diameters of 20–60 nm. The inset shows the initial part of the curves together with the experimental points recalculated from ref 22.

2) are at odds with both calibration curves and all experimental points. Surprisingly enough, we are now going to show that these points agree with Mie theory simulation.

Figure 3 shows experimental points of the works from refs 20, 25, 26, and 49 and Mie simulations based on the optical-constant splines Sp1, Sp2, and Sp3 with the real part $\Delta\varepsilon' = 0$ (Sp1-0, Sp2-0, and Sp3-0) and $\Delta\varepsilon' \neq 0$ (Sp1-1 and Sp2-1). First, we note that both sets, Sp1-1 and Sp2-1, do not describe the short-wavelength part of the experimental data for particle diameters $d \leq 20$ nm (see the inset in Figure 3), so those curves will not be considered further. It has been shown[20] that the anomalous behavior of the resonance peak position in the small-size region can be attributed to modification of the imaginary part of the dielectric function because of size-limiting effects. Second, our calculations with Sp1-0 constants (Otter's[38] data for 480–620 nm combined with eq 3) are in excellent agreement with Andreescu et al.'s[49] measurements, whereas both experimental sets[25,26] do not match the theoretical curve Sp1-0. However, calculations with Johnson and Christy's constants (curve Sp2-0) and Weaver et al.'s constants (spline curve Sp3-0) give better agreement with the measurements of the works of refs 25 and 26 and with our old experimental data.[20] Should this agreement be considered to be a strong confirmation of the validity of Mie simulations with Sp2-0 constants? We do not think so. Perhaps, the experimental data by Andreescu et al.[49] are in good agreement with Mie simulations because of spherical particle shape. As it has been pointed out by those authors,[49] their seed-mediated growth technology allowed fabrication of particles with extremely small deviations from spheres. This could explain a close agreement between the theoretical Sp1-0 curve and experimental points (unfortunately, there were no quantitative evaluations of the particle aspect ratio in the report[49]). Our previous analysis[20] showed that deviations of experimental points from the Mie curve are related (mainly) to particle nonsphericity and (less) to particle volume polydispersity. It follows from Figure 3 that our data[20] are in general agreement with both Haiss et al.'s[25] and Njoki et al.'s[26] measurements. Thus, we may conclude that disagreement between all three data sets[20,25,26] and the Sp1-0 curve can be explained by shape effects, whereas these shape effects were negligible in the experiments of Andreescu et al.[49]

To make our conclusion more convincing, we calculated the extinction peak position of gold s-cylinders and plotted the peak-position deviations from Mie theory $\Delta\lambda_{max}$ as a function of the particle aspect ratio (Figure 4). Clearly, we can expect significant red shifts caused by the particle shape even at moderate aspect ratios. To compare these calculations with experiment, we used the experimental data provided by Brown et al.[22] The inset shows experimental points recalculated from the data of ref 22 together with the initial part of the theoretical curves. Although there are quite appreciable quantitative differences between measurements and simulations, we may conclude that the experimental data confirm the expected shape-related shifts of Mie resonances.

It is evident from the inset in Figure 3 that the size of NPs with equivolume diameters smaller than 10 nm cannot be determined from the calibration curve or from eq 4 because of the anomalous behavior caused by the size-limiting effects. The small-particle region has been studied by Scaffardi et al.,[29,53] who proposed a NP-sizing method based on the dependence of the extinction contrast (A_{max}/A_{min}) on the average particle size $1 \leq d_{ev}(\text{nm}) \leq 10$, where $A_{min} \simeq A_{450}$. In fact, the same approach was used by Haiss et al. (see Figure 6b in ref 25) for an enlarged range of diameters, $3 \leq d_{ev}(\text{nm}) \leq 70$. Here, we extend consideration of the works of refs 25 and 29 to evaluate the shape effects on calibration of A_{max}/A_{min} vs particle size. Figure 5 shows the particle-size dependence of the extinction contrast A_{max}/A_{450}. Calculations were performed for gold s-cylinders with three aspect ratios $e = 1$, 1.2, and 1.4. In accordance with the previous observation,[29] the sensitivity of the calibration curve decreases strongly at diameters larger than 10–20 nm. However, the most important result is the quite small shape effects for all equivolume diameters less than 20 nm and aspect ratios less than 1.5. The inset in Figure 5 illustrates an exponential dependence of contrast on the particle diameter[25] and deviation from the exponential law

(53) Scaffardi, L. B.; Tocho, J. O. *Nanotechnology* **2006**, *17*, 1309–1315.

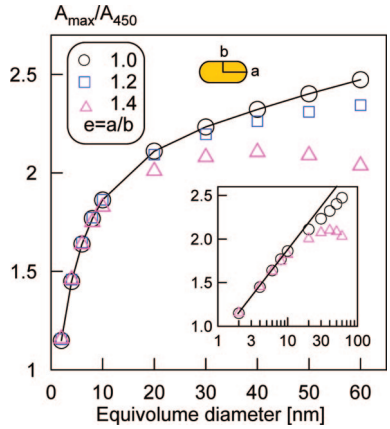

Figure 5. Calculated ratios of the extinction ratio A_{max}/A_{450} of gold s-cylinders, depending on their equivolume diameter and aspect ratio $e = 1$, 1.2, and 1.4. The inset shows linear fits for the logarithmic abscissa.

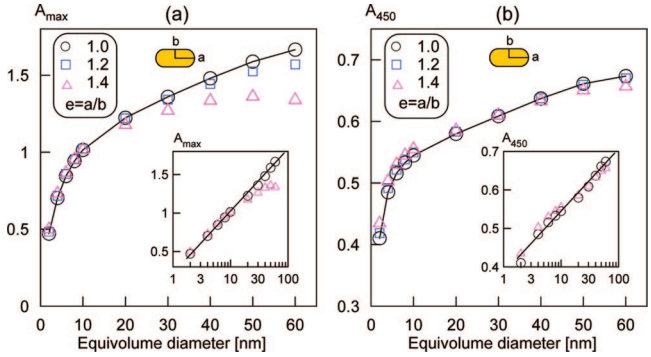

Figure 6. Calculated extinctions A_{max} (a) and A_{450} (b) of gold s-cylinders, depending on their equivolume diameter and aspect ratio $e = 1$, 1.2, and 1.4. The insets show linear fits for the logarithmic abscissa.

caused by particle shape. Thus, our simulations not only confirm the method used in refs 25 and 29 for spherical particles but extend its applicability to particles with moderate nonsphericity.

Now let us consider the concentration measurements by using absolute extinction measurements. In this context, two approaches are feasible: (1) measurements of the resonance extinction A_{max}[20] and (2) measurements of the short-wavelength extinction A_{450}.[25] Both approaches have been verified by Haiss et al.[25] in experiments with spherical particles. Figure 6 extends this approach to gold s-cylinders with small aspect ratios. Again, we note that the short-wavelength extinction A_{450} is almost insensitive to small variations in the particle shape, at least for diameters less than 60−80 nm. By contrast, the resonance extinction shows a notable deviation from the "spherical" curve, beginning with diameters of about 20−30 nm. Thus, for particles with significant deviations from spherical shape (e.g., for citrate particles[22]), concentration measurements using A_{450} instead of the resonance extinction A_{max} seem more preferable because of the smaller shape effects. On the other hand, the size-dependent slope of the resonance extinction curve is significantly greater than that in the case of A_{450} extinction. This fact means that determination of the concentration by resonance-extinction measurements may be more accurate than that with A_{450}, provided that all other things are equal.

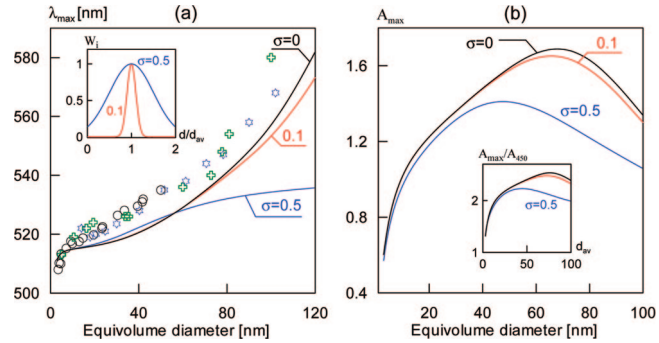

Figure 7. Position of the surface-plasmon-resonance peak (λ_{max}) (a) and the extinction-maximum values as functions of the average particle diameter of polydisperse NPs in water. Calculations for the normal weight distribution with polydispersity parameter $\sigma = 0$ (monodisperse particles), 0.1, and 0.3. The inset in panel a illustrates the corresponding distributions. The symbols designate experimental points taken from refs 20, 25, and 26 (circles, crosses, and stars, respectively). The inset in panel b shows the effect of polydispersity on the ratio A_{max}/A_{450}.

Finally, let us consider shortly the effects related to particle-size polydispersity. Regarding this point, we note an important recent study by Ji et al.,[54] who elucidated a new pH-mediated origin of colloidal gold polydispersity (citrate synthesis) and demonstrated a new route for the synthesis of nearly monodisperse gold NPs in the size range from 20 to 40 nm by simply varying the solution pH with fixed concentrations of $HAuCl_4$ and Na_3Ct. In accordance with typical experimental protocols, the total gold concentration c in our consideration is supposed to be constant. Therefore, the suspension polydispersity is expressed in terms of a distribution over the fraction weights w_i or over the mass-volume concentration c_i. It is easy to see that the suspension optical density A_{ext} is simply the sum of the weighed optical densities of fractions $w_i A_{ext,i}$, where

$$A_{ext,i} = \frac{3\lg(e)\, c w_i Q_{ext,i}}{4\pi R_{ev,i} l \rho_g} \qquad (5)$$

$Q_{ext,i}$ is the extinction efficiency of the ith fraction with an equivolume radius $R_{ev,i}$, l is the layer thickness, and ρ_g is the gold density. It should be emphasized that in the case of the particle number distribution $n_i = N_i/\sum N_i$, the total optical density would be equal to $\sum n_i A_{ext,i}$, with $A_{ext,i} = \lg(e) N \pi R_{ev,i}^2 Q_{ext,i}/l$, where N_i is the number of ith particles and N is the total number of particles per milliliter. Such averaging differs significantly from eq 5 and does not imply the total gold mass conservation for different distributions. That is why we do not consider it further. For the size polydispersity simulations, we choose a simple normal distribution with two standard parameters, d_{ev} and σ:

$$w_i \sim \exp[-(d_i/d_{av} - 1)^2/2\sigma^2] \qquad (6)$$

Figure 7 shows the spectral-maximum positions λ_{max}, the extinction maxima A_{max}, and the ratio A_{max}/A_{450} as functions of the mean equivolume diameter d_{av} of monodisperse particles ($\sigma = 0$), for a thin distribution ($\sigma = 0.1$), and for a broad distribution with $\sigma =$

(54) Ji, X.; Song, X.; Li, J.; Bai, Y.; Yang, W.; Peng, X. *J. Am. Chem. Soc.* **2007**, *129*, 13939–13948.

0.5 (see the inset in Figure 7). For comparison, we also reproduce three sets of experimental points taken from refs 20, 25, and 26. It is evident that a moderate size polydispersity ($\sigma < 0.1$) does not affect either the resonance peak positions or the resonance extinction, whereas for wide distributions, there are significant deviations from monodisperse curves at mean diameters larger than 60 nm. In any case, we conclude that polydispersity alone cannot explain the disagreement between calculated and measured peak positions.

In the case of polydisperse nonsperical particles, we have to introduce several parameters to describe the average particle size and shape, as well as the particle size and shape distribution. For simplicity, we adopt here a simplified model in which the s-cylinder thickness $2b$ is constant and determines the mean equivolume diameter $d_{av} = 2b[1 + 3(e_{av}-1)/2]^{1/3}$, whereas the particle aspect ratio e_i obeys the normal particle-weight distribution similar to that given by eq 5. Of course, variations in the particle length result in some kind of distribution over particle equivolume diameters d_i. Therefore, our model includes both size (d_i) and shape (e_i) distributions. Again, we stress that our simulations used particle-weight distribution rather than particle-number distribution. The calculated resonance-peak position and extinction maxima as a function of the averaged equivolume diameter are shown in Figure 8. The polydisperse nonspherical model fits the experimental data for the resonance wavelength, provided that the average aspect ratio and its variation are properly determined (in our case, $e_{av} = 1.3$ and $\sigma = 0.1$). Moreover, at moderate shape variations ($\sigma \leq 0.1$), we may neglect particle-shape polydispersity and may use a simpler monodisperse model with an averaged aspect ratio. The same is true for the extinction-maximum curve, unless the average aspect ratio is greater than 1.2−1.3. Otherwise, at $e_{av} = 1.5$, we observe a notable difference between the monodisperse and polydisperse models.

CONCLUSIONS

To summarize, we have shown that T-matrix simulations corrected for the mean electron free path afford a quantitative description of a long-term set of data on the particle-size dependence of the plasmon resonance position of gold NPs. We have also shown that both the size and the concentration of NPs can be accurately determined from UV−vis extinction spectra, provided that shape effects are taken into consideration. The size polydispersity of particles can be neglected in both T-matrix and Mie-theory simulations, unless the standard normal-distribution parameter σ is greater than 0.1. For larger polydispersities and for mean diameters greater than 20 nm, there appear significant deviations from simple monodisperse models. We believe that our discussion can help readers to understand possible limitations related to application of a simple monodisperse Mie model to determination of the size and concentration of gold NPs in laboratory samples.

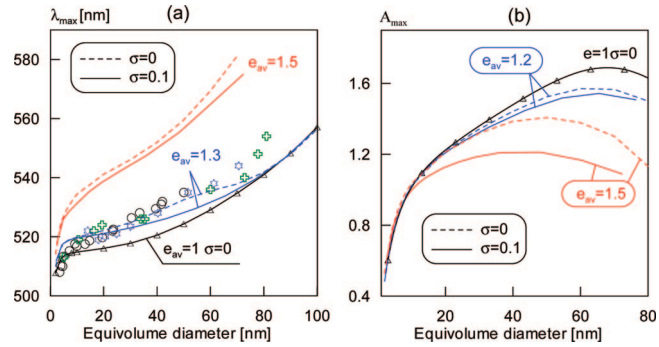

Figure 8. Dependences of the extinction-peak positions (a) and the extinction maxima (b) as a function of the mean equivolume diameter. T-matrix calculations for gold s-cylinders were performed with a normal distribution over the particle-aspect ratio with polydispersity parameters $\sigma = 0$ and 0.1 and the mean aspect ratios $e_{av} = 0$ (spheres), 1.2, 1.3, and 1.5.

ACKNOWLEDGMENT

This work was partly supported by grants from RFBR (Grant Numbers 08-02-00399a, 08-02-01074a, and 07-02-01434-a). The author thanks L. A. Dykman for help with the relevant literature and D. N. Tychinin for help in preparation of the manuscript.

Received for review April 25, 2008. Accepted June 18, 2008.

AC800834N